 doi:10.20944/preprints202109.0311.v1

Article

Copolymerization of quinazolinone derivatives with styrene, methyl methacrylate and their silver nanocomposites for biological applications

Karim S. El-Said[1,2*], Ahmed A. El-Barbary[3], Hazem M. ElKholy[3], Ahmed S. Haidyrah[4], Mohamed Betiha[5], Gaber El-Saber Batiha[6], Mohamed H. Mahmoud[7], Mohamed A. Abdelwahab[3]

1 Biochemistry Division, Chemistry Department, Faculty of Science, Tanta University, Tanta, Egypt

2 International Center for Materials Nanoarchitectonics, National Institute for Materials Science, Tsukuba, Ibaraki, Japan

3 Chemistry Department, Faculty of Science, Tanta University, Tanta, Egypt

4 Nuclear and Radiological Control Unit, King Abdulaziz City for Science and Technology, Riyadh, Saudi Arabia

5 Egyptian Petroleum Research Institute, Nasr City, Cairo, Egypt

6 Pharmacology and Therapeutics Department, Faculty of Veterinary Medicine, Damanhour University, Damanhour, AlBeheira, Egypt

7 Department of Biochemistry, College of Science, King Saud University, Riyadh, Saudi Arabia

*Correspondence: kareem.ali@science.tanta.edu.eg; Tel.: (+2) 01002977062

Abstract: Reaction of 2-mercapto-3-phenylquinazolin-4(3H)-one (MPQ) with both 4-vinyl benzyl chloride and allyl bromide furnished the reactive heterocyclic monomers 3-phenyl-2-((4-vinylbenzyl) thio) quinazolin-4(3H)-one (PVTQ) and 2-(allylthio)-3-phenylquinazolin-4(3H)-one (APQ), respectively. Copolymerization of PVTQ monomer with styrene and methyl methacrylate in the presence of 2,2'-azobisisobutyronitrile (AIBN) afforded the copolymers PS-co-PPVTQ and PMMA-co-PPVTQ, respectively. Similarly, copolymerization of monomer APQ with styrene and methyl methacrylate (MMA) afforded the copolymers PS-co-PAPQ and PMMA-co-PAPQ, respectively. The resulted copolymers were characterized by using FT-IR, 1H-NMR and GPC techniques. Silver nanocomposites of PS, PMMA, PS-co-PPVTQ, PMMA-co-PPVTQ, PS-co-PAPQ and PMMA-co-PAPQ were synthesized by the addition of silver nitrate into the polymer solution. The reduction of silver ions into silver nanoparticles was performed in DMF and water. Thermogravimetric (TGA) analysis was used to determine the thermal stability of the copolymers and their silver nanocomposites. The X-ray diffraction (XRD) analysis indicated the amorphous structures of the co-polymers and confirmed the formation of silver nanoparticles. The antitumor and antibacterial activities were screened for the copolymers and enhanced by the formation of their silver nanocomposites. In vivo antitumor activity in Ehrlich Ascitic Carcinoma (EAC) mice model showed that PS-co-PPVTQ/Ag NPs, PMMA-co-PPVTQ/Ag NPs, and PMMA-co-PAPQ/Ag NPs displayed promising inhibitory effects against EAC and induce apoptosis against MCF-7 cells.

Keywords: Quinazolinone; Styrene; Methacrylate; Nano-silver; Antibacterial; Antitumor.

1. Introduction

Synthesize of multifunctional macromolecular material showed a considerable interest for their potential usage in different polymer fields [1]. The radical homo-polymerization of benzocyclobuten-4-yl-acrylate and its copolymerization with styrene or n-butyl acrylate were carried out to produce the corresponding linear polymers, thermal analysis of the thermosetting systems suggests that they have potential use as high temperature macromolecular materials [2]. Co-polymerization of methyl methacrylate (MMA), glycidyl methacrylate (GMA) and the fluorinated monomer furnished the fluoropolymers showed high thermal stability, hydrophobicity, antifouling effect and antibacterial activity against Escherichia coli and Staphylococcus aureus [3]. Synthesis of 2,4,6-Trichlorophenyl methacrylate (TClPhMA) by the reaction of methacryloyl chloride with 2,4,6-trichlorophenol was copolymerized with monomers including styrene, 1,4-divinylbenzene and 2-hydroxymethyl methacrylate by bulk polymerization using benzoyl peroxide. These copolymers have potential application in polymer optical fiber technology due to their low refractive indices and high thermal resistance [4].

Preprints (www.preprints.org) | NOT PEER-REVIEWED | Posted: 17 September 2021 doi:10.20944/preprints202109.0311.v1

Anionic polymerization of p-(2,2′-diphenylethyl) styrene (DPES) monomers was achieved to afford well-defined block copolymer known as PDPES-b-PS. Radical polymerization of MMA in the presence of DPES effectively afforded a graft copolymer composed of a polystyrene backbone and PMMA branches [5]. Furthermore, the homopolymers of 2,4-dichlorophenyl methacrylate and its copolymers with 8-quinolinyl methacrylate (8-QMA) were prepared. The presence of 2,4-dichlorophenyl methacrylate led to inhibition of microorganism growth [6]. Phenylethyl acrylate (PEA) and 2-Phenylethyl methacrylate (PEMA) were synthesized by reacting 2-Phenyl ethanol with acryloyl- and methacryloyl chloride, respectively. Copolymers of PEA and PEMA with methyl acrylate and N-vinyl pyrrolidone (NVP) of different compositions were prepared and tested on leather for their pressure sensitive adhesive property [7]. By free radical polymerization, 8-acryloxyquinoline (8-AQ) monomer was prepared through the reaction of 8-hydroxyquinoline with either acryloyl chloride or acrylic acid in the presence of triethylamine or N, N-dicyclohexylcarbodiimide. The antimicrobial activity of all compounds demonstrated moderate to good activity against the tested strains providing wider possibilities for the synthesis of pharmacologically active polymers [8]. Improved polymerizations of monomers bearing electron transporting substituents based on 2,5-diphenyloxadiazole and 2,3-diphenylquinoxaline attached directly to a vinyl group were reported, these materials have been incorporated into light emitting polymer devices in which hole conduction properties are provided by 4-vinyltriphenylamine groups for usage in optimized devices [9].

Preparation and structural analysis of poly (styrene-co-acrylic acid) composite nanospheres (PSA) and silver nanoparticles (Ag-NPs) loaded PSA was reported, the Ag-NPs were well-dispersed on the surfaces of PSA composite nanospheres by in situ chemical reduction of AgNO3 [10]. A modified method based on in situ chemical reduction was developed to prepare mono-dispersed polystyrene/silver (PS/Ag) composite microspheres. With the addition of $[Ag(NH_3)_2]^+$ to the PS dispersion, $[Ag(NH_3)_2]^+$ complexions were absorbed and reduced to Ag-NPs on the surfaces of PS-PDA microspheres to form PS/Ag composite microspheres [11]. The green PS/AgNPs nanocomposite exhibited antimicrobial activity against Gram-negative and Gram-positive bacteria that showed a potential application in food packaging [12]. Additionally, it has been reported that of silver polystyrene sulfonate polyelectrolyte showed promising biomedical applications [13]. The PS/Ag composite microspheres were prepared successively by addition of $[Ag(NH_3)_2]+$ complex ions to the templates dispersion, adsorbing to the surfaces of templates, and then reduction of $[Ag(NH_3)_2]+$ complex ions to Ag-NPs. These PS/Ag composite microspheres showed potent catalytic properties [14]. This study aimed to synthesis copolymers of quinazolinone derivatives with styrene, methyl methacrylate and their silver nanocomposites and evaluate their antibacterial and anticancer activities. The importance of the present work lies in the possibility that the polymers and their conjugates might be more efficacious antibacterial and antitumor agents, which could be helpful in designing more potent drugs for therapeutic use.

2. Materials and Methods

2.1. Chemicals

Styrene (ST), methyl methacrylate (MMA), 4-vinyl benzyl chloride, allyl bromide, 2,2′-azobisisobutyronitrile (AIBN), and silver nitrate were purchased from Sigma Aldrich and used as received. Cisplatin (Cis) was purchased from local pharmacy in Egypt and diluted to 2mg/kg for mice injection.

Preprints (www.preprints.org) | NOT PEER-REVIEWED | Posted: 17 September 2021 doi:10.20944/preprints202109.0311.v1

2.2. Methods

2.2.1. Synthesis of 3-phenyl-2-thioxo-2,3 dihydroquinazolin-4(1H)-one (MPQ) [15].

Anthranilic acid (27 g, 200 mmol) and 23.85 mL (200 mmol) of phenyl isothiocyanate were refluxed in anhydrous pyridine (30 mL) for 5 h. (tlc). The reaction was cooled to r.t. and the solvent was evaporated till dryness under vacuum. The solid product was crystallized from methanol, m.p. 310-312 ^{o}C and yield 95 %.

2.2.2. Synthesis of 3-phenyl-2-((4-vinylbenzyl) thio) quinazolin-4(3H)-one (PVTQ).

Compound MPQ (5.0 g, 19.7 mmol) was dissolved in methanol (30 mL) and 0.79 g (19.7 mmol) of NaOH, to which 2.99 g (3.94 mmol) of 4-vinyl benzyl chloride was added. The reaction mixture was stirred at r.t. for 2 h (tlc) and the resulted solid was separated by filtration and crystallized from methanol, m.p. 160-162 ^{o}C and yield 69 %. FTIR (Figure 1A) (film on KBr plate): v (cm-1) 3057 (ar. C-H), 1691 (st.C=O), 1609 (st. C=C), 1543 (C=N). MS. (EI) m/z = 370.22 (M+, $C_{23}H_{18}N_2OS$, 70.16 %). Analysis for $C_{23}H_{18}N_2OS$ (270.11) Calcd: C, 74.57%; H, 4.90%; N, 7.56%. Found: 74.39%; 4.78%; 7.70%.

2.2.3. Synthesis of 2-(allylthio)-3-phenylquinazolin-4(3H)-one (APQ) [16].

Compound MPQ (5.0 g, 19.7 mmol) was dissolved in methanol (30 mL) and 0.79 g (19.7 mmol) of NaOH, to which 2.34 g (3.94 mmol) of allyl bromide was added. The reaction mixture was stirred at r.t. for 2 h (tlc) and the resulted solid was separated by filtration and crystallized from methanol, m.p. 150-152 ^{o}C and yield 80 %. FTIR (Figure 1B) (film on KBr plate): v (cm^{-1}) 3060 (ar. C-H), 2977, 2931 (aliph. C-H), 1678 (st. C=O), 1606 (st. C=C), 1444 (st. C=N). Analysis for $C_{17}H_{14}N_2OS$ (294.08) Calcd: C, 69.36%; H, 4.79%; N, 9.52%. Found: 69.60%; 5.01%; 10.00%.

2.2.4. Copolymerization of compound PVTQ with styrene and/or methylmethacrylate to form copolymers (PS-co-PPVTQ) and (PMMA-co-PPVTQ).

Compound PVTQ (0.5 g, 1.35 mmol), 1 mL of St. (8.74 mmol) and/or MMA (9.40 mmol) and 0.01 g (0.061 mmol) of AIBN were heated for 5 h till solidification. The resulted solids were dissolved in $CHCl_3$ (30 mL) and precipitated by pouring on a large amount of methanol to furnish the copolymers PS-co-PPVTQ and PMMA-co-PPVTQ, respectively.

2.2.5. Polystyrene-co-poly(3-phenyl-2-((4-vinylbenzyl)thio)quinazolin-4(3H)-one) (PS-co-PPVTQ).

FTIR (Figure 1A) (film on KBr plate): v (cm-1) 3025 (ar. C-H), 2926, 2851 (aliph. C-H), 1691 (st.C=O), 1615 (st. C=C), 1544 (C=N). ^{1}H-NMR (CDCl3) (Figure 2): δ (ppm) = 1.411-1.540 (br. 4H, CH2), 1.820 (br. 2H, CH), 4.342 (s, 2H, SCH_2), 6.458-8.260 (m, CH ar).

2.2.6. PolyMMA-co-poly(3-phenyl-2-((4-vinylbenzyl)thio)quinazolin-4(3H)-one) (PMMA-co-PPVTQ).

FTIR (Figure 1A) (film on KBr plate): v (cm^{-1}) 2995, 2946 (aliph. C-H), 1735 (st. C=O of PMMA), 1686 (st. C=O of quinazolinone moiety), 1612 (st. C=C), 1546 (C=N). ^{1}H-NMR (CDCl3) (Figure 2): δ (ppm) = 0.619-1.032 (br. 4H, CH_2 of PMMA), 1.550 (s, 3H, CH_3C), 1.825-1.859 (br. 2H, CH_2CH), 2.743-2.752 (br. 1H, CH), 3.607 (s, 3H, CH_3O), 4.345 (s, 2H, SCH2) 6.919-8.252 (m, CH ar).

2.2.7. Copolymerization of compound APQ with styrene and/or methylmethacrylate to form the copolymers PS-co-PAPQ and PMMA-co-PAPQ.

Preprints (www.preprints.org) | NOT PEER-REVIEWED | Posted: 17 September 2021 doi:10.20944/preprints202109.0311.v1

Compound APQ (0.5 g, 1.70 mmol), 1 mL of St (8.74 mmol) and/or MMA (9.40 mmol) and 0.01 g (0.061 mmol) of AIBN were heated for 5 h till solidification. The resulted solids were dissolved in $CHCl_3$ (30 mL) and precipitated by pouring on a large amount of methanol to furnish the PS-co-PAPQ and PMMA-co-PAPQ, respectively.

2.2.8. Polystyrene -co- poly (2-(allylthio)-3-phenylquinazolin-4(3H)-one)(PS-co-PAPQ).

FTIR (Figure 1A) (film on KBr plate): v (cm-1) 3066, 3026 (ar. C-H), 2921, 2853 (aliph. C-H), 1696 (st. C=O), 1600 (st. C=C), 1548 (C=N). ^{1}H-NMR ($CDCl_3$) (Figure 3): δ (ppm) = 1.131-1.528 (br. 4H, CH_2), 1.857-2.078 (br. 2H, CH), 3.849-3.873 (d, 2H, SCH_2), 6.406-7.563 (m, CH ar).

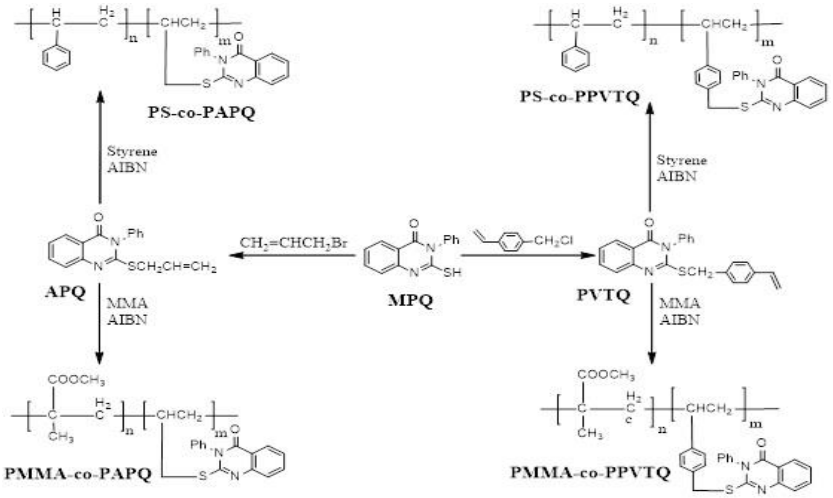

Scheme 1. Synthesis of linear copolymers PS-co-PPVTQ, PMMA-co-PPVTQ, PS-co-PAPQ and PMMA-co-PAPQ.

2.2.9. PolyMMA -co- poly (2-(allylthio)-3-phenylquinazolin-4(3H)-one) (PMMA-co-PAPQ).

FTIR (Figure 1A) (film on KBr plate): v (cm-1) 3001 (ar. C-H), 2952 (aliph. C-H), 1730 (st. C=O of two interfered carbonyl groups of PMMA and quinazolinone moiety), 1635 (st. C=C), 1551 (C=N). ^{1}H-NMR ($CDCl_3$) (Figure 3): δ (ppm) = 0.755-0.945 (br. 3H, $CHCH_2$), 1.835 (br. 2H, CH_2C), 2.501 (s, 3H, CH_3C), 3.320 (s, 3H, CH_3O) 3.403-3.562 (d, 2H, SCH_2), 6.348-8.252 (m, CH ar).

2.2.10. General procedure for preparation of silver nanocomposites of PS, PMMA and PS-co-PPVTQ, PMMA-co-PPVTQ, PS-co-PAPQ and PMMA-co-PAPQ.

PS, PMMA, PS-co-PPVTQ, PMMA-co-PPVTQ, PS-co-PAPQ and/or PMMA-co-PAPQ (0.5 g, 90 wt%) were dissolved in DMF (20 mL) to which 0.056 g (10 wt%) of silver nitrate was added. The reaction mixtures were stirred at r.t for 2 h followed by heating at 90 °C for 6 h. until brown color was observed. The reaction mixtures were cooled, and the products were precipitated by pouring the mixtures on a large amount of methanol, filtered off and dried in vacuum oven at 40 °C for 2 days.

2.3. Characterization

All melting points were uncorrected and performed by the open capillary melting point apparatus. FT-IR spectra were recorded on Bruker, Tensor 27FT-IR spectrophotometer with frequency range 4000cm^{-1} to 400cm^{-1} (Central Lab, Tanta University, Egypt) with KBr pellets and 4 cm-1 resolutions. Elemental analyses were determined on Heraeus (Microanalysis Center, Cairo University, Giza, Egypt). 1H-NMR spectra were measured on a

Preprints (www.preprints.org) | NOT PEER-REVIEWED | Posted: 17 September 2021 doi:10.20944/preprints202109.0311.v1

Varian mercury VX-300 (300 MHz) NMR spectrometer (Nuclear Magnetic Resonance lab., Faculty of science, Cairo University, Cairo, Egypt). The mass spectra (MS) were recorded on GCMS/QP 1000 Ex mass spectrometer at 70 eV (Microanalysis Center, Cairo University, and the National Research Centre, Dokki, Giza, Egypt). The TGA data were obtained by using shimadzu thermal analyzer system at a heating rate of 5 ^{o}C/min, sample weight of 5-6 mg under nitrogen (20 mL/min) flow. The range investigated from 30-400 ^{o}C (The Central Lab, Tanta University, Egypt). The XRD measurements were carried out using GRN, APD 2000 PRO X-Ray diffraction, equipped with a Ni-filtered Cu-Kα radiation (λ= 1.54 Å) at a scanning rate of 0.05°/s and divergent slit 0.3 (Central Lab. Tanta University, Egypt).

2.4. Determination of antibacterial activity

For antibacterial screening, a stock solution of 5 mg of quinazolinone derivatives, their copolymers and copolymers/Ag NPs were dissolved in 1 mL of dimethyl sulfoxide (DMSO) and graded quantities of the test compounds were incorporated in specified quantity of molten sterile agar (nutrient agar, 28 g/L, pH=7.4). The media were sterilized in autoclave before experiment and poured into a Petri dish to give a depth of 3-4 mm and allowed to solidify. Suspension of the microorganism was prepared to contain approximately 5 × 10−5 cfu/mL. The culture plates were seeded with test organisms. Uniform wells were created, filled with 100 µL of the test compounds and incubated at 37 °C for 24 h. DMSO was used as a control with zero inhibition zone [17, 18].

2.5. In vivo anticancer studies using Ehrlich Ascetic Carcinoma (EAC) model

Female Swiss albino mice weighting 20 ± 2 g were obtained from National Research Center (NRC, Cairo, Egypt). Mice were kept for a week before starting the experiment for adaptation at the Animal Facility, Zoology Department, Faculty of Science, Tanta University. The experimentation, transportation and care of the animals were performed and handled in compliance with the ethical guidelines approved by the animal care and use committee, Faculty of Science, Tanta University (ACUC-SCI-TU-103), Egypt and according to the National Institutes of Health guide for the care and use of Laboratory animals (NIH Publications No. 8023, revised 1996). EAC cells were collected in sterile 0.9% saline from the tumor bearing mice. The viable and dead EAC cells were counted using trypan blue method and the number was adjusted at 2×10^{6} cells/mouse for inoculation. Total viable cells were calculated as following: Mean number of unstained cells × dilution × 10^{4}/ml. Eighty female Swiss albino mice were divided into ten groups (n = 8). All groups were inoculated i.p with 2×10^{6} (EAC) cells/mouse and after 24 hours, Gp2 had treated with Cisplatin reference anticancer drug (2 mg/kg), Gp3-10 had treated with PS-co-PPVTQ, PMMA-co-PPVTQ, PS-co-PAPQ, PMMA-co-PAPQ, PS-co-PPVTQ/Ag NPs, PMMA-co-PPVTQ/Ag NPs, PS-co-PAPQ/Ag NPs, and PMMA-co-PAPQ/Ag NPs (10 mg/kg), respectively, daily for six consecutive days. On day 14, all groups were sacrificed to assess the tumor volume, count, and live/dead cells.

2.6. In vitro cytotoxic effect by MTT assay

To determine the anticancer activity of the synthesized copolymers/nanocomposites in vitro, MTT assays were used to on MCF-7 cells, the tested polymers were dissolved in dimethyl sulfoxide (DMSO) and diluted with saline to the appropriate concentration. Different concentrations (from 200 to 3.125 µg/mL) of these compounds were applied in triplicate to the MCF-7 cells (at 70–80% confluent in Dulbecco's modified Eagle medium), and the wells were incubated, then, 10 µL of a 12 mM MTT stock solution [5 mg/mL MTT in sterile phosphate buffered saline (PBS)] was added to each well. This was followed by incubation for 4 h at 37 °C. The MTT solution was removed, and the purple formazan crystal formed at the bottom of the wells was dissolved with 100 µL of DMSO for 20 min. Cisplatin (Cis) was used as a positive standard. The absorbance at 570 nm was read on an

Preprints (www.preprints.org) | NOT PEER-REVIEWED | Posted: 17 September 2021 doi:10.20944/preprints202109.0311.v1

enzyme-linked immunosorbent assay reader (StatFax-2100, Awareness Technology, Inc.). The concentration of thecompounds inhibiting 50% of cells (IC_{50}) was calculated with the sigmoidal curve.

2.7. Statistical analysis

Data expressed as means ± S.D. that were analyzed by One–way analysis of variance (ANOVA) was used to assess the significant differences among treated groups. $p < 0.05$ was considered as a significant value for all statistical analyses.

3. Results and discussion

3.1. Synthesis, FTIR, ^{1}H-NMR and MS Characterizations

The FITR spectra of compounds PVTQ and APQ showed C=O at 1691, 1678, C=C at 1609 and 1606 cm^{-1}, respectively (Figure 1A and B). MS of compound PVTQ displayed m/z at 370.22 which corresponding to molecular ion peak (M^+, $C_{23}H_{18}N_2OS$) with relative abundance 70.16 %. Copolymerization of compound PVTQ with styrene and/or MMA furnished copolymers PS-co-PPVTQ and PMMA-co-PPVTQ, respectively. FITR spectrum of copolymer PS-co-PPVTQ revealed stretching aliphatic CH at 2926, 2851 and C=O at 1691cm^{-1} as shown in Fig 1A. ^{1}H-NMR spectrum exhibited a broad methylene (CH_2) proton at 1.411-1.540 (protons b, d), a broad methine (CH) protons at 1.820 (protons a, c), a singlet SCH_2 protons at 4.342 (protons e) and multiple aromatic protons at 6.458-8.260 ppm (Figure 2).

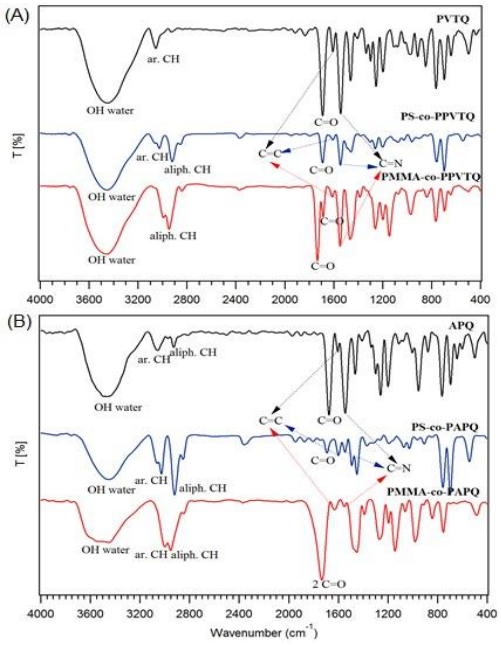

Figure 1. FTIR spectra **(A)** Compound **PVTQ**, copolymers PS-co-PPVTQ and PMMA-co-PPVTQ. **(B)** Compound APQ, copolymers PS-co-PAPQ and PMMA-co-PAPQ.

FITR spectrum of copolymer PMMA-co-PPVTQ showed stretching aliphatic CH at 2995, 2946 and two C=O at 1735 (PMMA) and 1686 (quinazolinone moiety) cm^{-1} (Figure 1A). Its ^{1}H-NMR spectrum displayed broad methylene (CH_2) protons of PMMA at 0.619-1.032 (protons c), singlet methyl (CH_3C) protons at 1.550 (protons a), a broad CH_2CH protons at 1.825-1.859 (protons e), a broad methine (CH) protons at 2.743-2.752 (protons d),

Preprints (www.preprints.org) | NOT PEER-REVIEWED | Posted: 17 September 2021 doi:10.20944/preprints202109.0311.v1

singlet methyl (CH_3O) protons at 3.607 (protons b), a singlet SCH_2 protons at 4.345 (protons f) and a multiplet aromatic protons at 6.919-8.252 ppm (Figure 2).

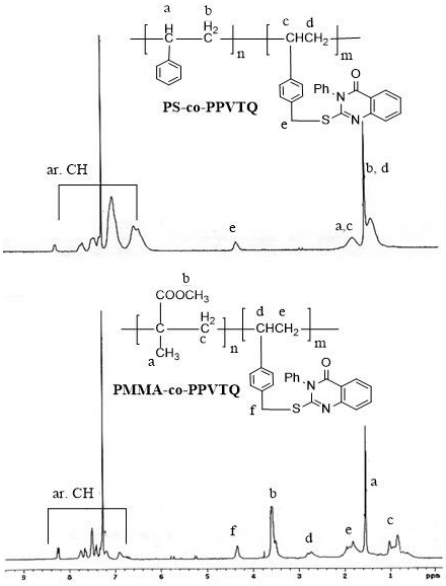

Figure 2. ^{1}HNMR spectra of copolymers PS-co-PPVTQ and PMMA-co-PPVTQ.

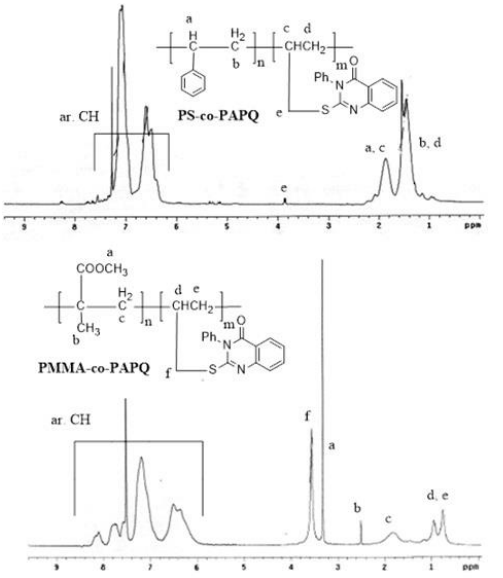

Figure 3. ^{1}H-NMR spectra of copolymer PS-co-PAPQ and PMMA-co-PAPQ.

Copolymerization of compound APQ with styrene and/or MMA furnished copolymers PS-co-PAPQ and PMMA-co-PAPQ, respectively. FITR spectrum of copolymer PS-co-PAPQ exhibited stretching aliphatic CH at 2921, 2853 and C=O at 1696 cm^{-1} as shown in Fig 1B. ^{1}H-NMR spectrum revealed a broad CH_2 protons at 1.131-1.528 (protons b, d), a broad CH proton at 1.857-2.078 (protons a, c), a doublet SCH_2 protons at 3.849-3.873 (protons e) and a multiplet aromatic protons at 6.406-7.563 ppm (Figure 3).

FITR spectrum of copolymer PMMA-co-PAPQ showed stretching aromatic CH at 3001, aliphatic CH at 2952 and C=O at 1730 cm^{-1} that may be referred to the overlapped carbonyl groups of PMMA and quinazolinone moieties as shown in Fig 1B. ^{1}H-NMR spectrum displayed a broad CH_2CH protons at 0.765-0.945 (protons d and e), a broad CH_2C protons at 1.835 (protons c), a singlet CH_3C protons at 2.501 (protons b), a singlet CH_3O protons at 3.320 (protons a), a doublet SCH_2 protons at 3.403-3.562 (protons f) and a multiplet aromatic protons at 6.348-8.252 ppm (Figure 3).

3.2. Thermogravimetric Analysis (TGA)

Thermal degradation and the thermal stability of copolymers PS, PMMA, PS-co-PPVTQ, PMMA-co-PPVTQ, PS-co-PAPQ, PMMA-co-PAPQ and their Silver nanocomposites were investigated using TGA and DTG as shown in Figures. 4, 5 and Table 1. T_{10} and T_{50} represent the temperatures at which weight change can be detected with 10 % and 50 % of weight loss, respectively. T_P represents the temperature of maximum rate of degradation. DTG curves showed that the thermal degradation of PS, PS/Ag NPs, PS-co-PPVTQ, PS-co-PAPQ and PS-co-PAPQ/Ag NPs occurred in one-step degradation at T_P indicating random scission of the polymer chains. The thermal degradation of PS-co-PPVTQ/Ag NPs occurs in two-step degradations with close temperatures indicating

 doi:10.20944/preprints202109.0311.v1

random scission decomposition of hetero moieties followed by the polymer chains. This may be due to the coordination binding of silver nanoparticles with the hetero atoms in the polymer chains.

According to decomposition temperatures at T_{10}, T_{50} and T_p of PS, PS/Ag NPs, they nearly have the same thermal stability. PS-co-PPVTQ, PS-co-PAPQ and PS-co-PPVTQ/Ag NPs decomposition temperatures at T_{10} and T_{50} are lower than the corresponding values of PS. Thus, we can conclude that PS-co-PPVTQ, PS-co-PAPQ and PS-co-PPVTQ/Ag NPs are less thermally stable than PS. In addition, PS-co-PAPQ/Ag NPs decomposition temperatures at T_{10} and T_{50} are higher than the corresponding values of PS and PS-co-PAPQ. Thus, PS-co-PAPQ/Ag NPs is more thermally stable than PS and PS-co-PAPQ. This may be due to the presence of hetero moieties through the polymer chain and the distribution and bonding of silver nanoparticles along the polymer hetero atoms [19].

Table 1. TGA data of PS, PMMA, PS-co-PPVTQ, PMMA-co-PPVTQ, PS-co-PAPQ and PMMA-co-PAPQ.

Compound	T_{10}	T_{50}	T_p	R_{650} (%)
PS	352	400	408	0.00
PS/Ag NPs	351	396	405	1.32
PS-co-PPVTQ	320	386	415	0.00
PS-co-PAPQ	345	398	411	0.00
PS-co-PPVTQ/Ag NPs	335	383	401	1.36
PS-co-PAPQ/Ag NPs	373	409	415	1.14
PMMA	282	338	374	0.00
PMMA/Ag NPs	282	345	375	1.11
PMMA-co-PPVTQ	315	389	435	0.00
PMMA-co-PAPQ	327	372	380	0.00
PMMA-co-PPVTQ/Ag NPs	313	367	369	1.10
PMMA-co-PAPQ/Ag NPs	302	365	376	1.12

The DTG curves showed that the thermal degradation of PMMA, PMMA/Ag NPs and PMMA-co-PAPQ/Ag NPs occurred in two-steps degradation. The first degradation is attributed to the decomposition of PMMA unsaturated chain ends and the second degradation is related to random scission of the polymer chains [20]. Additionally, the thermal degradation of PMMA-co-PPVTQ, PMMA-co-PAPQ and PMMA-co-PPVTQ/Ag NPs occurred in one-step degradation indicating random scission of the polymer chains. According to decomposition temperatures at T_{10} and T_{50} of PMMA, PMMA/Ag NPs, they nearly have the same thermal stability. PMMA-co-PPVTQ, PMMA-co-PAPQ, PMMA-co-PPVTQ/Ag NPs and PMMA-co-PAPQ/Ag NPs decomposition temperatures at T_{10} and T_{50} are higher than the corresponding values of PMMA and PMMA/Ag NPs. Thus, they are more thermally stable than PMMA and PMMA/Ag NPs. This may be due to the presence of hetero moieties through the polymer chain, the distribution and bonding of silver nanoparticles along the polymer hetero atoms.

The comparison of T_{10} and T_{50} decomposition temperatures of PMMA-co-PPVTQ with PMMA-co-PPVTQ/Ag NPs and PMMA-co-PAPQ with PMMA-co-PAPQ/Ag NPs displays that PMMA-co-PPVTQ/Ag NPs and PMMA-co-PAPQ/Ag NPs are less thermally stable than PMMA-co-PPVTQ and PMMA-co-PAPQ, respectively. So, the addition of silver to PMMA-co-PPVTQ and PMMA-co-PAPQ decreases their thermal stability. From TGA curves, the content of silver metal nanoparticles in PS/Ag, PS-co-PPVTQ/Ag, PS-co-

Preprints (www.preprints.org) | NOT PEER-REVIEWED | Posted: 17 September 2021 doi:10.20944/preprints202109.0311.v1

PAPQ/Ag, PMMA/Ag, PMMA-co-PPVTQ/Ag, PMMA-co-PAPQ/Ag composites is estimated to be 1.32, 1.36, 1.14, 1.11, 1.10 and 1.12 %, respectively.

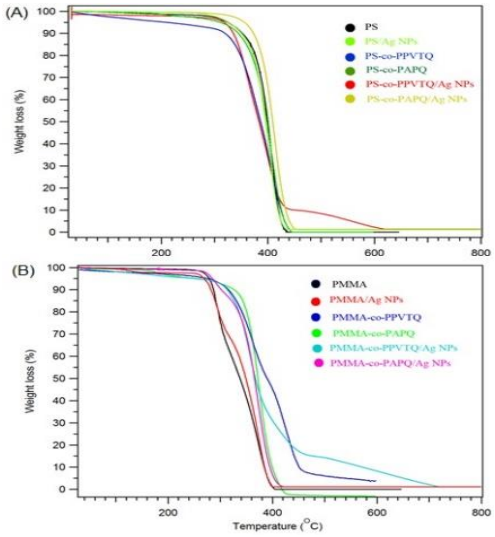

Figure 4. (A) TGA of PS, PS-co-PPVTQ, PS-co-PAPQ and their silver nanoparticles. **(B)** TGA of PMMA, PMMA-co-PPVTQ, PMMA-co-PAPQ and their silver nanoparticles.

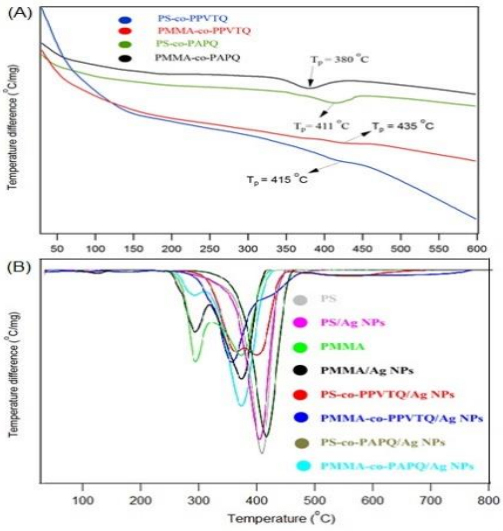

Figure 5. (A) DTG of PS-co-PPVTQ, PS-co-PAPQ, PMMA-co-PPVTQ, PMMA-co-PAPQ. **(B)** DTG of PS, PS/Ag, PMMA, PMMA/Ag, PS-co-PPVTQ/Ag, PS-co-PAPQ/Ag, PMMA-co-PPVTQ/Ag and PMMA-co-PAPQ/Ag NPs.

3.3. X-ray diffraction

The X-ray diffraction patterns of PMMA-co-PPVTQ, PMMA/Ag NPs, PMMA-co-PPVTQ/Ag NPs, PS-co-PAPQ, PS/Ag NPs and PS-co-PAPQ/Ag NPs (Figure 6). Previous study showed that silver nanoparticles exhibited peaks at 2θ angles of 38.1˚, 44.3˚, 64.4˚, 77.4˚ and 81.5˚ corresponding to the reflections of the (111), (200), (220), (311) and (222) crystal plane of the face-centered cubic (fcc) structure of Ag [10, 11]. The strong reflections of PS-co-PPVTQ and PMMA-co-PPVTQ around 2θ = 18.95˚ and 15.55˚, respectively are assigned to their amorphous structures. XRD of PS/Ag NPs, PS-co-PPVTQ/Ag NPs, PMMA/Ag NPs, and PMMA-co-PPVTQ/Ag NPs displayed the same previous peaks that referred to amorphous structure and indicated to the formation of silver nanoparticles with the appearance of Ag reflections peaks at 32.35˚, 38.10˚, 43.95˚, 64.25˚ and 77.60˚. Similarly, XRD of PS-co-PAPQ/Ag NPs and PMMA-co-PAPQ/Ag NPs displayed the same previous peaks that referred to amorphous structure and indicated to the formation of silver nanoparticles with the appearance of Ag reflections peaks at 38.15°, 44.40˚ and 75.65˚. The weak intensity of silver nanoparticles peaks may be referred to the small amount of reduced silver ions. It further confirmed that silver nanoparticles with crystallinity could be obtained successfully by reducing of $AgNO_3$ using DMF and water on the surface of the polymers under study [21].

Preprints (www.preprints.org) | NOT PEER-REVIEWED | Posted: 17 September 2021 doi:10.20944/preprints202109.0311.v1

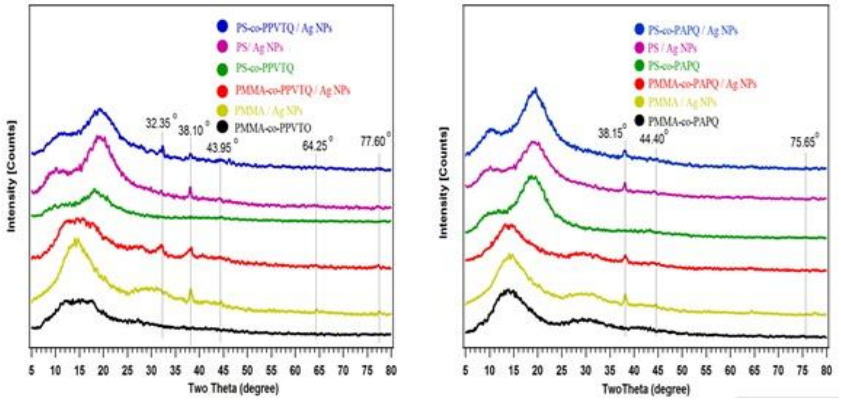

Figure 6. XRD analysis of copolymers and their silver nanocomposites.

3.4. Antibacterial activity

Using polymeric nanoparticles and nanocomposites as controlled drug delivery systems have attracted great attention due to their high drug loading capacity and ability to release the loaded drug in controlled fashion [22]. Table 2 and Figure 7 showed the antibacterial activity against some Gram-positive and Gram-negative bacteria using agar cup plate method, ciprofloxacin was used as standard drug [23]. Compound PVTQ, copolymers PS-co-PPVTQ, PMMA-co-PPVTQ, PS-co-PAPQ and PMMA-co-PAPQ showed a negative inhibition zones towards all types of bacteria under study. Compound APQ showed a high inhibition zone (20 mm) according to the standard drug (21 mm) towards *Klebsiella pneumoniae* and negative results for other types of bacteria. Thus, the copolymerization of compounds PVTQ and APQ with styrene and methyl methacrylate does not affect all types of bacteria under study. Addition of silver nanoparticles to PS, PS-co-PPVTQ, PMMA-co-PPVTQ, PMMA, PS-co-PAPQ and PMMA-co-PAPQ resulted in a significant increase in the inhibition zones compared with copolymers PS-co-PPVTQ, PMMA-co-PPVTQ, PS-co-PAPQ and PMMA-co-PAPQ. Inhibition zones of PS-co-PPVTQ/Ag NPs, PS-co-PAPQ/Ag NPs, PMMA-co-PPVTQ/Ag NPs, and PMMA-co-PAPQ/Ag NPs were enhanced compared with PS/Ag NPs and PMMA/Ag NPs. This may be due to the presence of heterocyclic moieties (PVTQ and APQ) in the copolymer chain and Ag NPs. This increase in inhibition zones is referred to the accumulation of Ag NPs in the bacterial cell membrane caused a change in the permeability, structural and morphological changes that resulting in cell death [12]. As the silver nanoparticles contact with the bacteria, they agglutinate to the cell wall and membrane [24]. Once bound, some silver exceeds inside and combines with phosphate moieties of DNA and RNA, while another portion adheres to the sulfur-containing proteins on the membrane [24]. At the membrane, silver-sulfur interactions cause structural variations and pores formation in bacterial cell wall [25]. Through these pores, cellular components are freed into the extracellular fluid due to the osmotic difference. Through the cell, the presence of silver creates a low molecular weight region where DNA condenses [25]. The condensed DNA inhibits the cell's replication proteins contact with the DNA. Thus the introduction of Ag NPs inhibits replication and cause cell death [25,26].

Preprints (www.preprints.org) | NOT PEER-REVIEWED | Posted: 17 September 2021 doi:10.20944/preprints202109.0311.v1

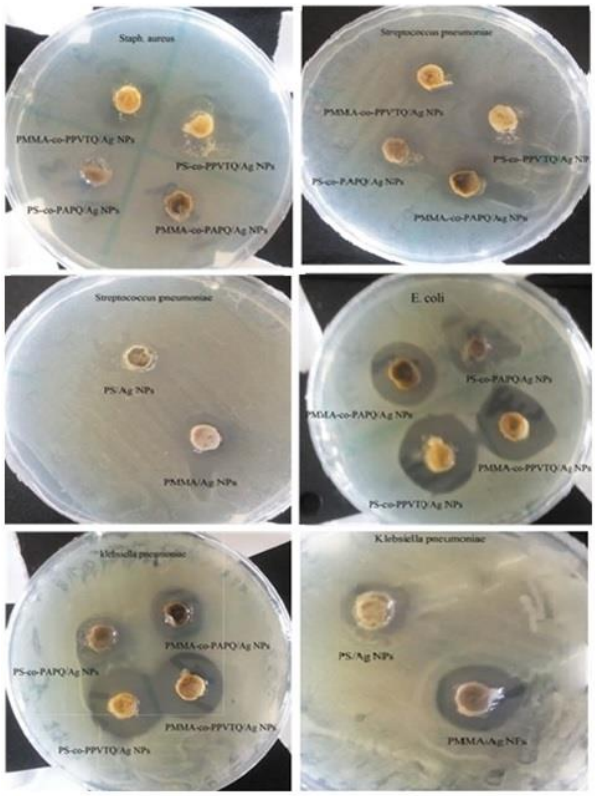

Figure 8. Antibacterial activity of copolymers and their silver nanocomposites.

Table 2. Antibacterial activity of the different co-polymers/nanocomposites.

	Inhibition zone diameter (mm)			
Compounds/Bacterial strain	**S. aureus**	**S. pneumoniae**	**E. coli**	**K. pneumoniae**
Ciprofloxacin	19	24	22	21
PVTQ	00	00	00	00
PS-co-PPVTQ	00	00	00	00
PMMA-co-PPVTQ	00	00	00	00
APQ	00	00	00	20
PS-co-PAPQ	00	00	00	00
PMMA-co-PAPQ	00	00	00	00
PS/Ag NPs	00	00	00	14
PS-co-PPVTQ/Ag NPs	21	19	23	22
PMMA-co-PPVTQ/Ag NPs	20	15	22	23
PMMA/Ag NPs	10	13	12	18
PS-co-PAPQ/Ag NPs	11	11	14	13
PMMA-co-PAPQ/Ag NPs	16	13	20	16

Preprints (www.preprints.org) | NOT PEER-REVIEWED | Posted: 17 September 2021 doi:10.20944/preprints202109.0311.v1

3.5. In vivo anticancer activity using carcinoma mice model

Synthetic polymers, biopolymers, and their nanocomposites have been widely applied in different medical areas particularly in cancer therapy, owing to their desired mechanical and physical properties, manufacturability into various shapes, sterilizing capability, and ease of modification with multiple functionalities [27, 28]. Development of such these materials require high standards regarding their biocompatibility, functionality, and bioactivity [29]. The synthesized copolymers and/or their silver nanocomposites in this study were evaluated as anticancer agents using EAC mice model. Each compound was injected as a concentration of 10 mg/kg daily for consecutive 6 days starting from day 0. For comparison, cisplatin (Cis) used as standard reference anticancer drug an evaluated under the same conditions, which injected as 2mg/kg for consecutive 6 days. Tumor profile including the total EAC volume, count, and viability of copolymers and/or their silver nanocomposites and Cis are shown in Table 3. It was evident that the promising compounds that displayed EAC tumor growth inhibition can be order as the following PMMA-co-PPVTQ/Ag NPs > PMMA-co-PAPQ/Ag NPs > PS-co-PPVTQ/Ag NPs > PS-co-PAPQ/Ag NPs > PMMA-co-PPVTQ > PMMA-co-PAPQ, when compared to EAC-bearing mice control. These findings were agreed with previous study evaluated the antitumor efficacy of some biocompatible polymers and nanocomposites [17, 18, 30, 31].

Table 3. Antitumor activity of the different co-polymers/nanocomposites. Total EAC volume, count, and viability of the different groups under study

Groups	Total EAC volume (×10⁶/mouse)	Total EAC count (×10⁶/mouse)	Total viable EAC count (×10⁶/mouse)	Total dead EAC count (×10⁶/mouse)
Gp1	11.5 ± 0.9a*	498 ± 6.8a*	496 ± 6.3a*	2 ± 0.25a*
Gp2	0.35 ± 0.15b*	52 ± 2.3b*	29 ± 2.7b*	23 ± 1.2b*
Gp3	9.5 ± 1.2 a*	474 ± 8.1a*	462 ± 9.2a*	12 ± 3.9a*
Gp4	8 ± 1.3c*	465± 9.8c*	449 ± 9.1c*	16 ± 3.1c*
Gp5	10 ± 1.5a*	484 ± 7.5a*	480 ± 8.a*	4 ± 0.57a*
Gp6	9 ± 1.35a*	480 ± 8.1a*	472 ± 8.2a*	9 ± 2.9 a*
Gp7	7.2 ± 0.95c*	458 ± 9c*	440 ± 7.9c*	18 ± 3.1c*
Gp8	5 ± 1.0d*	404 ± 7.8d*	372 ± 9.1d*	32 ± 5.2d*
Gp9	7.9 ± 1.0c*	460 ± 9.8c*	443 ± 8.1c*	17 ± 6.9c*
Gp10	6.2 ± 1.8d*	423 ± 6.8d*	403 ± 7.1d*	20 ± 4.5d*

Gp1: EAC-bearing mice, Gp2: EAC/Cis, Gp3: EAC/PS-co-PPVTQ, Gp4: EAC/PMMA-co-PPVTQ, Gp5: EAC/PS-co-PAPQ, Gp6: EAC/PMMA-co-PAPQ, Gp7: EAC/PS-co-PPVTQ/Ag NPs, Gp8: EAC/PMMA-co-PPVTQ/Ag NPs, Gp9: EAC/PS-co-PAPQ/Ag NPs, Gp10: EAC/ PMMA-co-PAPQ/Ag NPs. * Means that do not share a letter are significantly different.

3.6. In vitro anticancer activity

Polymeric nanoparticles protect against *in vitro* and *in vivo* degradation. Besides synthetic biopolymers and their nanocomposites prepared by a macromolecular matrix have attracted great attention in recent years for several medical and non-medical applications due to their outstanding properties [31]. Polymer nanocomposites have significant potential in disease theranostics, and nanotechnology brings great promise in cancer drug carriers [32]. The cytotoxicity of the copolymers/nanocomposites was evaluated *in vitro* against the MCF-7 cells. The IC_{50} values of the PHB–thiol polymers and reference anticancer drug (Cis) are shown in Table 4. It was evident that the tested copolymers and their nanocomposites showed cancer-cell-growth inhibition. The most promising compounds can be ordered as the following PMMA-co-PAPQ/Ag NPs > PMMA-co-PPVTQ/Ag NPs > PS-co-PAPQ/Ag NPs > PMMA-co-PPVTQ > PS-co-PPVTQ/Ag NPs, with IC_{50} values ranging from 38.6 to 54.3 µg/ml as compared to the Cis Among all tested compounds, the most promising composites is PMMA-co-PAPQ/Ag NPs that showed IC_{50} value of 38.6 µg/ml. However, PS-co-PPVTQ showed the lowest cytotoxic inhibitory effect, with an IC_{50} value of 83.4 µg/ml. PS-co-

Preprints (www.preprints.org) | NOT PEER-REVIEWED | Posted: 17 September 2021 doi:10.20944/preprints202109.0311.v1

PPVTQ/Ag NPs composites showed a moderate cytotoxic effect against MCF-7 ells showing IC_{50} value of 54.3 µg/ml (Table 4). These findings were agreed with previous studies reported the effectiveness of copolymers and/or their nanocomposites in inhibition of cancer growth, copolymer based on tri (ethylene glycol)-methyl ether methacrylate and [10 -(2-acryloxy)-3,30 -dimethyl-6-nitrospiro-(2H-1-benzopyran-2,20 -indoline)] has proven its effectiveness in the case of cancer therapy [33-35].

Table 4. IC_{50} Values of the cytotoxic effects of copolymers/nanocomposites and standard Cisplatin on the MCF7 cell lines

Compound	IC_{50} (µg/ml)
Cisplatin	19.2
PS-co-PPVTQ	83.4
PS-co-PAPQ	76.5
PS-co-PPVTQ/Ag NPs	54.3
PS-co-PAPQ/Ag NPs	50.7
PMMA-co-PPVTQ	51.1
PMMA-co-PAPQ	62.7
PMMA-co-PPVTQ/Ag NPs	40.13
PMMA-co-PAPQ/Ag NPs	38.6

3. Conclusion

Some copolymers of quinazolinone derivatives with styrene and methyl methacrylate were successfully prepared and their chemical structures were elucidated using FT-IR and 1H-NMR techniques. The formation of silver nanoparticles with the prepared copolymer was performed in DMF and water using silver nitrate. The thermal stability and degradation of copolymers and their silver nanocomposites were evaluated through TGA and XRD. The synthesized copolymers showed no antibacterial activity towards the biological species so, their antibacterial activity was enhanced by the formation of silver nanoparticles on the surface of copolymers. Furthermore, in vivo, and in vitro antitumor activity in mice model showed that PS-co-PPVTQ/Ag NPs, PMMA-co-PPVTQ/Ag NPs, and PMMA-co-PAPQ/Ag NPs have the most promising inhibitory effects against tumor growth.

Author Contributions: Conceptualization, K.S.-E; data curation, writing—review, resources, editing, methodology, visualization, A.A.-E.; supervision, validation, H.M.-E and M.B..; software, investigation, methodology, formal analysis, A.S.-H, G.E-B., and M.H.-M; data curation, project administration, funding acquisition and M.A.-A.; methodology, software, writing—original draft preparation, formal analysis. All authors have read and agreed to the published version of the manuscript

Funding: This work was funded through Researchers Supporting Project number (RSP-2021/406), King Saud University (Riyadh, Saudi Arabia)

Institutional Review Board Statement: The study was conducted in compliance with the ethical guidelines approved by the animal care and use committee, Faculty of Science, Tanta University (ACUC-SCI-TU-103), Egypt and according to the National Institutes of Health guide for the care and use of Laboratory animals (NIH Pub-lications No. 8023, revised 1996).

Informed Consent Statement: Informed consent was obtained from all subjects involved in the study.

Data Availability Statement: Data sharing not applicable.

Acknowledgments: The authors would like to extend their gratitude to King Saud University (Riyadh, Saudi Arabia) for the funding of this research through Researchers Supporting Project number (RSP-2021/406)

Conflicts of Interest: All authors declare no conflict of interest.

References

1. Arun, A.; Reddy, B. 1, 4-pentadien-3-one-1-p-hydroxyphenyl-5-p-phenyl acrylate: Crosslinking studies and reactivity ratios with glycidyl methacrylate. *Poly. Res.* **2004**, *11*, 195–201.
2. Xie, L.; Yang, J.; Zhu, F.; Yang, H.; Liu, C.; Zhang, L. Synthesis and characterization of benzocyclobuten-4-yl acrylate monomer and its radical polymerization. *Chinese J. Poly. Sci.* **2010**, *28*, 877–885.
3. Zhu, P.; Meng, W.; Huang, Y. Synthesis and antibiofouling properties of crosslinkable copolymers grafted with fluorinated aromatic side chains. *RSC Adv.* **2017**, *7*, 3179–3189.
4. Demirci, G.; Podkościelna, B.; Bartnicki, A.; Mergo, P.; Gil, M.; Cetinkaya, O.; Gawdzik, B. Copolymerization and thermal study of the new methacrylate derivative of 2, 4, 6-trichlorophenol. *Ther. Anal. Calor.* **2017**, *127*, 2263–2271.
5. Huang, M.; Han, B.; Lu, J.; Yang, W.; Fu, Z. Anionic polymerization of p-(2, 2′-diphenylethyl) styrene and applications to graft copolymers. *Desig. Mono. Poly.* **2017**, *20*, 66–73.
6. Patel, P.; Shah, B.; Ray, A.; Patel, R. Acrylic Homo-and Co-polymers Based on 2, 4-dichlorophenyl Methacrylate and 8-quinolinyl Methacrylate. *Poly. Res.* **2004**, *11*, 65–73.
7. Senthilkumar, U.; Ganesan, K.; Reddy, B. Synthesis, characterization and reactivity ratios of phenylethyl acrylate/methacrylate copolymers. *Poly. Res.* **2003**, *10*, 21–29.
8. Khalil, A. Activated polymers. II: Synthesis and exchange reactions of biologically active poly (8-acryloxyquinoline). *Poly. Res.* **2013**, *20*, 28.
9. Dailey, S.; Feast, W.J.; Peace, R.J.; Sage, I.C.; Till, S.; Wood, E.L. Synthesis and device characterisation of side-chain polymer electron transport materials for organic semiconductor applications. *Mat. Chem.* **2001**, *11*, 2238–2243.
10. Zhang, J.; Zhao, X.; Wang, Y.; Zhu, L.; Yang, L.; Li, G.; Sha, Z. Preparation and structural analysis of nano-silver loaded poly (styrene-co-acrylic acid) core-shell nanospheres with defined shape and composition. *Nanomat.* **2017**, *7*, 234.
11. Zhu, W.; Wu, Y.; Yan, C.; Wang, C.; Zhang, M.; Wu, Z. Facile synthesis of mono-dispersed polystyrene (PS)/Ag composite microspheres via modified chemical reduction. *Mat.* **2013**, *6*, 5625–5638.
12. Awad, M.A.; Mekhamer, W.; Merghani, N.M.; Hendi, A.A.; Ortashi, K.M.; Al-Abbas, F.; Eisa, N.E. Green synthesis, characterization, and antibacterial activity of silver/polystyrene nanocomposite. *Nanomat.* **2015**, *2015*, 5.
13. Girard, J.; Brunetto, P.S.; Braissant, O.; Rajacic, Z.; Khanna, N.; Landmann, R.; Daniels, A.U.; Fromm, K.M. Development of a polystyrene sulfonate/silver nanocomposite with self-healing properties for biomaterial applications. *Comptes. Rend. Chimie.* **2013**, *16*, 550–556.
14. Yougen, H.; Tao, Z.; Pengli, Z.; Rong, S. Preparation of monodisperse polystyrene/silver composite microspheres and their catalytic properties. *Coll. Poly. Sci.* **2012**, *290*, 401–409.
15. Alafeefy, A.M. Some new quinazolin-4 (3H)-one derivatives, synthesis, and antitumor activity. *Saudi Chem. Soci.* **2011**, *15*, 337–343.
16. Hagar, M.; Soliman, S.M.; Ibid, F.; El Sayed, H. Synthesis, molecular structure and spectroscopic studies of some new quinazolin-4 (3H)-one derivatives; an account on the N-versus S-Alkylation. *Mol. Struc.* **2016**, *1108*, 667–679.

17. Abdelwahab, M.; El-Barbary, A.; El-Said, K.; Betiha, M.; Elkholy, H.; Chiellini, E.; El-Magd, M. Functionalization of poly (3-hydroxybutyrate) with different thiol compounds inhibits MDM2–p53 interactions in MCF7 cells. *Appl. Poly. Sci.* **2019**, *136,* 46924.

18. Abdelwahab, M.A.; Ahmed, A.; El-Said, K.S.; El Naggar, S.A.; ElKholy, H.M. Evaluation of antibacterial and anticancer properties of poly (3-hydroxybutyrate) functionalized with different amino compounds. *Int. J. Biol. Macrom.* **2019**, *122,* 793–805.

19. Pozdnyakov, A.; Emel'yanov, A.; Ermakova, T.; Prozorova, G. Functional polymer nanocomposites containing triazole and carboxyl groups. *Poly. Sci. Series B.* **2014**, *56,* 238–246.

20. Valandro, S.R.; Lombardo, P.C.; Poli, A.L.; Horn, M.A.; Neumann, M.G.; Cavalheiro, C.C.S. Thermal properties of poly (methyl methacrylate)/organomodified montmorillonite nanocomposites obtained by in situ photopolymerization. *Mat. Res.* **2014**, *17,* 265–270.

21. Pacioni, N.L.; Borsarelli, C.D.; Rey, V.; Veglia, A.V. Synthetic routes for the preparation of silver nanoparticles. *Silver Nanop. App.* **2015**, 13–46.

22. Kim, D.K.; Dobson, J.J. Nanomedicine for targeted drug delivery. *Mater Chem.* **2009**, *19,* 6294–6307.

23. Appani, R.; Bhukya, B.; Gangarapu, K. Synthesis and Antibacterial Activity of 3-(Substituted)-2-(4-oxo-2-phenylquinazolin-3 (4H)-ylamino) quinazolin-4 (3H)-one. *Scientifica.* **2016**, Article ID 1249201, 5.

24. Klasen, H. A historical review of the use of silver in the treatment of burns. II. Renewed interest for silver. *Burns.* **2000**, *26,* 131–138.

25. Feng, Q.L.; Wu, J.; Chen, G.; Cui, F.; Kim, T.; Kim, J. A mechanistic study of the antibacterial effect of silver ions on Escherichia coli and Staphylococcus aureus. *Biomed. Mat. Res.* **2000**, *52,* 662–668.

26. Sankar, R.; Karthik, A.; Prabu, A.; Karthik, S.; Shivashangari, K.S.; Ravikumar, V. Origanum vulgare mediated biosynthesis of silver nanoparticles for its antibacterial and anticancer activity. *Colloids and Surfaces B: Biointer.* **2013**, *108,* 80–84.

27. Bordat, A.; Boissenot, T.; Nicolas, J.; Tsapis, N. Thermoresponsive polymer nanocarriers for biomedical applications. *Adv. Drug Deliv. Rev.* **2019**, *138,* 167–192.

28. Li, S.; Chang, K.; Sun, K.; Tang, Y.; Cui, N.; Wang, Y.; Qin, W.; Xu, H.; Wu, C. Amplified singlet oxygen generation in semiconductor polymer dots for photodynamic cancer therapy. ACS Appl. *Mater. Interf.* **2016**, *8,* 3624–3634.

29. da Silva, D.; Kaduri, M.; Poley, M.; Adir, O.; Krinsky, N.; Shainsky-Roitman, J.; Schroeder, A. Biocompatibility, biodegradation and excretion of polylactic acid (PLA) in medical implants and theranostic systems. *Chem. Eng.* **2018**, *340,* 9–14.

30. Salahuddin, N.; Elbarbary, A.A.; Alkabes, H.A. Antibacterial and anticancer activity of loaded quinazolinone polypyrrole/chitosan /silver chloride nanocomposite. *Int. J. Polym. Mater. Polym. Biomater.* **2017**, *66,* 307–316.

31. Feldman, D. Polymers and polymer nanocomposites for cancer therapy. *Appl. Sci.* **2019**, *9,* 3899.

32. Thakur, S.; Pramod, K.S.; Malviya, R. Utilization of polymeric nanoparticle in cancer treatment. A Review. *Pharm. Care Health Syst.* **2017**, *4,* 1–12.

33. Zou, H.; Liu, H. Synthesis of thermal and photo dual-responsive amphiphilic random copolymer via atom transfer radical polymerization and its control release of doxorubicin. *Int. J. Polym. Mater. Polym. Biomater.* **2017**, *66,* 955–962.

34. Solairaja, D.; Rameshthangama, P.; Arunachalam, G. Anticancer activity of silver and copper embedded chitin nanocomposites against human breast cancer (MCF-7) cells. *Int. J. of Biol. Macromol.* **2017**, *105,* 608–619.

35. Janitabar-Darzi, S.; Rezaei, R.; Yavari, K. In vitro cytotoxicity effects of 197Au/PAMAMG4 and 198Au/PAMAMG4 nanocomposites against MCF7 and 4T1 breast cancer cell lines. *Adv. Pharm. Bull.* **2017**, *7,* 87–95.